

# Molecular Dynamics of High-Pressure Liquid Water: Going from Ambient to Near-Critical Temperatures

Ioannis Skarmoutsos<sup>\*,[a]</sup> and Elvira Guardia<sup>[b]</sup>

The properties of high-pressure liquid water were investigated along the isobar of 25 MPa and in the temperature range 298.15–623.15 K using classical molecular dynamics simulations. Particular attention has been given to the changes in the local structural and related dynamic properties of liquid water. The results obtained have revealed noticeable changes in the shape of the calculated radial distribution functions, as well as the existence of local extrema or crossovers in several structural descriptors and entropic quantities at temperatures around 423.15 K and

498.15 K, where also significant changes in the hydrogen bond network of liquid water have also been observed. The temperature dependence of translational, reorientational, and hydrogen bond dynamics of liquid water has also been investigated by calculating the translational self-diffusion and the corresponding O-H vector Legendre reorientational correlation times and hydrogen bond lifetimes. The corresponding activation energies for each investigated relaxation process have also been presented and discussed.

## 1. Introduction

High-temperature, pressurized liquid water is a commonly used medium in several processes employed to destroy hazardous chemicals, as well as in a wide range of chemical reactions.<sup>[1–5]</sup> It is also considered a green solvent for several extraction processes of organic molecules, with particular emphasis on the extraction of natural products.<sup>[6–11]</sup> Due to the significant changes in the polarity of high-temperature water, it is also used as the mobile phase in the so-called “superheated water chromatography”, replacing reversed-phase high-performance liquid chromatography with conventional organic solvents.<sup>[12]</sup>

All these applications are closely related to the changes in the physicochemical properties of liquid water when going from ambient to high temperature and pressure conditions.<sup>[13]</sup> However, in order to provide a deeper insight into the effect of temperature and pressure on the properties of liquid water, a molecular-scale understanding of these phenomena becomes indispensable. Among the different methods employed to investigate the molecular-scale processes taking place in liquid water, molecular simulation techniques<sup>[14]</sup> are considered a very powerful computational tool. Molecular simulation is regarded as the link between theory and experiment and sheds light on a wide

range of phenomena taking place on the microscopic, molecular scale.

In this respect, the main aim of the present work is to employ molecular dynamics (MD) simulation techniques in order to investigate the temperature effect on the thermodynamic, structural, and dynamic properties of liquid water along a high-pressure isobar (25 MPa), where several chemical and industrial applications take place. Using the well-known TIP4P-2005 potential model of water,<sup>[15]</sup> which provides reliable predictions of the phase diagram and many properties of water in a very wide range of thermodynamic conditions, MD simulations were employed to investigate liquid water along the 25 MPa isobar and in the temperature range 298.15–623.15 K. Particular emphasis has been given to the changes in the local hydrogen bonding (HB) network in water and the corresponding local structural features of high-pressure liquid water, as reflected on several local structural order parameters previously proposed in the literature.<sup>[16,17]</sup> Moreover, the entropic phenomena associated with these structural changes have been also presented, together with the corresponding changes in the translational and reorientational dynamics of the water molecules as the temperature increases.

The manuscript has been organized as follows: The computational methodology is presented in Section II, the results and discussion in Section III, and the conclusions are summarized in Section IV.

## 2. Computational Details


In the framework of the present study, a series of classical MD simulations of liquid water along the  $P = 25$  MPa isobar and in a wide temperature range (298.15 – 623.15 K, using a temperature interval  $dT = 25$  K) have been employed. The simulated systems consisted of 500 water molecules, which were placed inside cubic simulation boxes, using also periodic boundary conditions.

[a] I. Skarmoutsos

Laboratory of Physical Chemistry, Department of Chemistry, University of Ioannina, Ioannina 45110, Greece  
E-mail: [iskarmoutsos@uoi.gr](mailto:iskarmoutsos@uoi.gr)

[b] E. Guardia

Departament de Física, Universitat Politècnica de Catalunya, Campus Nord-Edifici B4-B5, Jordi Girona 1–3, Barcelona E-08034, Spain

 © 2025 The Author(s). Chemistry – A European Journal published by Wiley-VCH GmbH. This is an open access article under the terms of the [Creative Commons Attribution-NonCommercial-NoDerivs](https://creativecommons.org/licenses/by-nc-nd/4.0/) License, which permits use and distribution in any medium, provided the original work is properly cited, the use is non-commercial and no modifications or adaptations are made.

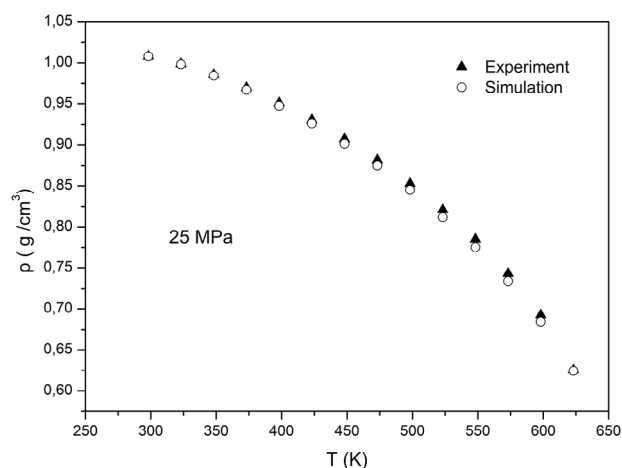


**Figure 1.** Calculated and experimental temperature dependence of the density of liquid water along the 25 MPa isobar.

The initial configurations were constructed using the Packmol software.<sup>[18]</sup> Each system was equilibrated for 5 ns at the NPT ensemble and the densities were estimated from subsequent 5 ns NPT-MD runs. Using the values of the calculated densities of the system, subsequent NVT-MD runs of 5 ns were performed to re-equilibrate each system, followed by 5 ns production runs to extract the systems' properties. The well-known TIP4P-2005 potential model of water<sup>[15]</sup> was used in the simulations. Note that the predicted critical temperature of water from previously reported molecular simulations<sup>[19]</sup> using the TIP4P-2005 model is  $T_c = 640$  K, ensuring that even at the highest investigated temperature (623.15 K) simulated water is still in the liquid state.

In all MD simulations, the equations of motion in the simulations were integrated using a leapfrog-type Verlet algorithm<sup>[14]</sup> and the integration time step was set to 1 fs. The intramolecular geometry of all the simulated species was constrained using the quaternion formalism. A Nose–Hoover thermostat<sup>[20]</sup> and barostat,<sup>[21]</sup> with corresponding temperature and pressure relaxation times of 0.2 and 0.5 ps, respectively, were used to constrain the temperature and the pressure during the simulations. A 9 Å cutoff was used to treat the van der Waals interactions, using analytical tail corrections, while the long-range electrostatic interactions were treated using the standard Ewald summation method.<sup>[14]</sup> All the simulations were performed using the DL\_POLY simulation code<sup>[22]</sup> and the simulation trajectories were analyzed using Fortran codes developed by the authors to calculate the properties of the simulated systems.

### 3. Results and Discussion

The calculated density of liquid water along the isobar of 25 MPa as a function of temperature is presented in Figure 1, where an excellent agreement with available experimental data<sup>[23]</sup> can be observed. As the temperature increases, a significant non-linear decrease of the density is observed and at near critical temperatures (623.15 K), the density of water has decreased by about 38% in comparison with its value at ambient temperature (298.15 K), with the latter having the value of  $1.008 \text{ g cm}^{-3}$ .

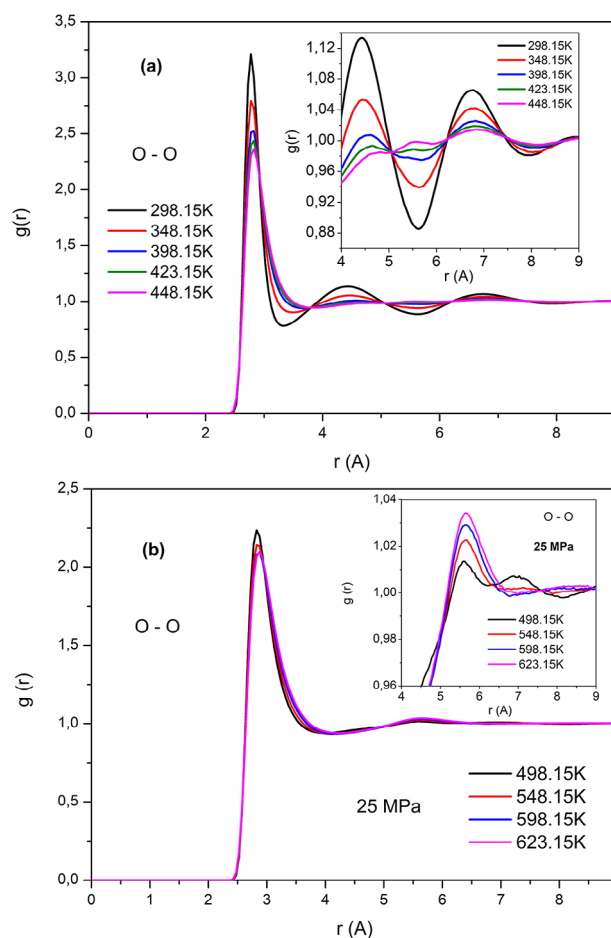


**Figure 2.** Temperature dependence of the calculated O-O RDF.

The density changes as the temperature increases are also reflected upon the local intermolecular structure of liquid water, as it can also be observed in Figure 2, where the temperature dependence of the O-O radial distribution functions (RDF) along the 25 MPa isobar is presented. As it can be seen in Figure 2a, at near-ambient temperatures the O-O RDF exhibits a clear second and third peak and corresponding minima, which are very characteristic for near-ambient liquids<sup>[24–26]</sup> and indicate the formation of a second and third solvation shell. The first peak intensity of the O-O RDF decreases as the temperature increases, however, this decrease is much less pronounced at temperatures higher than 498.15 K, as it can be clearly observed in Figure 2b. The shape of the calculated O-O RDF is also in agreement with the experimental measurements of Soper, who performed neutron diffraction experiments and empirical potential structure refinement at 423 K and 10 MPa and also at 573 K and 10 and 50 MPa.<sup>[27]</sup> Moreover, the location of the first minimum of the O-O RDF, which determines the radius of the first solvation shell, shifts to longer intermolecular distances as the temperature increases. For instance, the first minimum of the O-O RDF at 298.15 K is located at 3.3 Å, and at 623.15 K the position of the first minimum has shifted to 4.2 Å.

As the temperature increases, the intensity of the second and third peaks drastically decreases as well. As it can be clearly seen in the inset picture in Figure 2a, in the temperature range

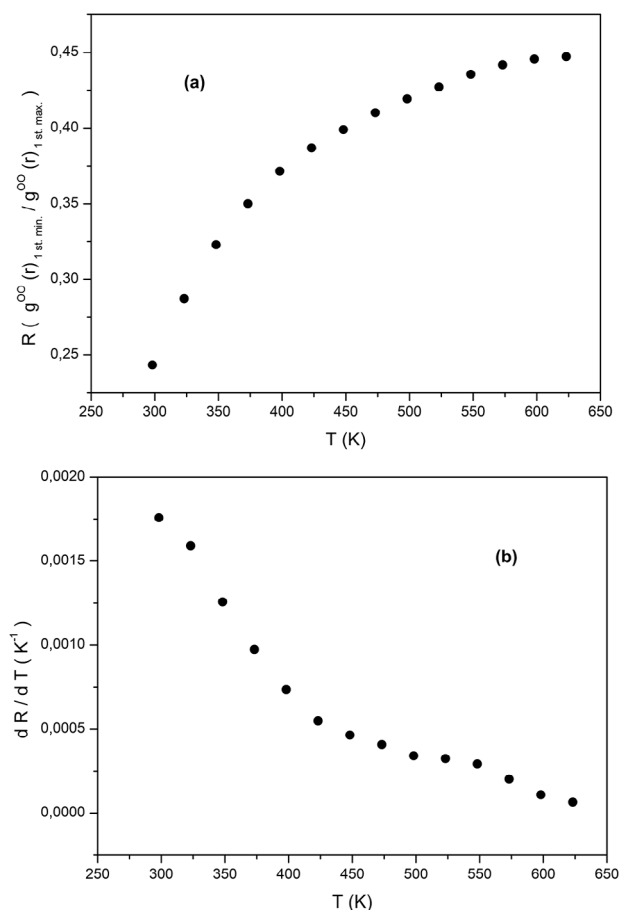


**Figure 3.** Temperature dependence of the calculated Wendt-Abraham parameter  $R$  and its derivative  $dR/dT$ .

298.15–398.15 K the second peak intensity decreases with the increase of the temperature, and the position of this peak slightly shifts to longer distances. In the temperature range 423.15 – 473.15 K, this second peak splits to a shoulder located at about 4.7 Å and another peak at 5.5 Å, whereas the third peak is located at 6.8 Å. Finally, at 498.15 K the shoulder observed in the temperature range 423.15 – 473.15 K vanishes, whereas at higher temperatures the third peak also vanishes. Note also that at temperatures higher than 498.15 K the intensity of the second peak increases with the increase of the temperature, whereas the second minimum shifts to longer distances, around 6.8 Å. All these features clearly indicate that at temperatures higher than 423.15 K the intermolecular structure in liquid water along the 25

MPa isobar starts to change and at temperatures higher than 498.15 K, it exhibits significant differences with the liquid structure observed at ambient temperature. This is more clearly reflected in the behavior of the Wendt-Abraham parameter  $R$ ,<sup>[28]</sup> which is defined as the ratio between the first minimum and maximum intensities of the O-O RDF, respectively:

$$R = \frac{g^{OO}(r)_{1st\ min}}{g^{OO}(r)_{1st\ max}} \quad (1)$$

The bulk density dependence of the Wendt-Abraham parameter  $R$ , as well as its derivative  $dR/dT$ , are presented in Figure 3.

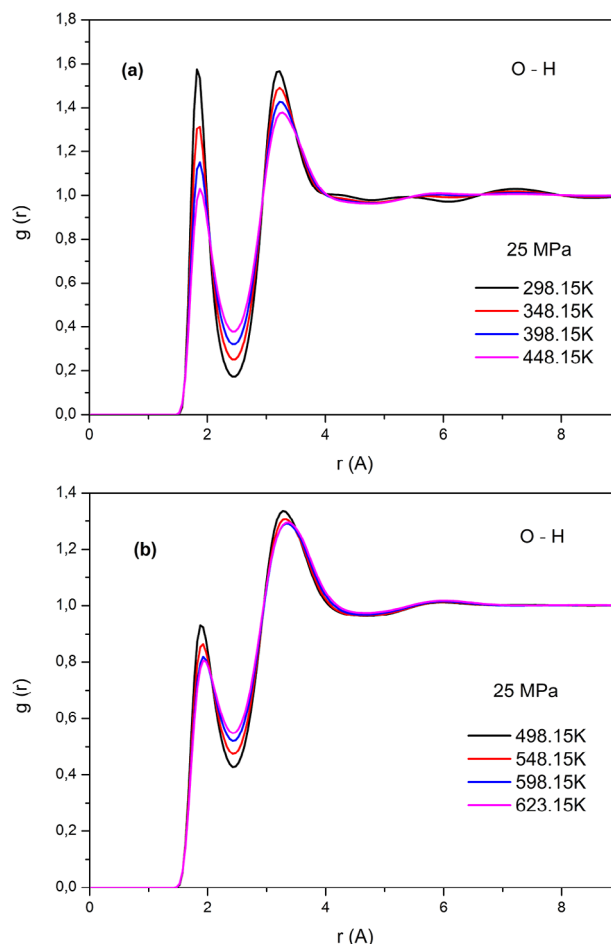


**Figure 4.** Temperature dependence of the calculated O-H RDF.

Especially from the temperature dependence of  $dR/dT$ , depicted in Figure 3b, three different regions can be observed. The first region corresponds to temperatures lower than 423.15 K, the second to the temperature range 423.15–523.15 K, and the last region to temperatures higher than 523.15 K. All these findings are clearly in line with the previous observations regarding the changes in the shape of the O-O RDF and the corresponding structural transitions in liquid water along the 25.0 MPa isobar.

Regarding the shape of the O-H RDF, presented in Figure 4, as the temperature increases the first peak intensity decreases and the first minimum intensity increases for the whole temperature range investigated. The positions of the first maximum and minimum are not significantly affected by the temperature changes and they are located around 1.85 and 2.45 Å, respectively. Note also that at ambient temperature the intensities of the first and second peaks, with the latter located around 3.3 Å, are almost similar. However, as the temperature increases the intensity of the first peak becomes clearly lower than the one corresponding to the second one. The shape of the calculated O-H RDF also indicates the existence of hydrogen bonds formed between the water molecules. In order to provide a quantitative description of the changes in the HB network of water as the temperature increases, a commonly used geometric criterion<sup>[29–34]</sup> was employed in our analysis. According to this criterion, a

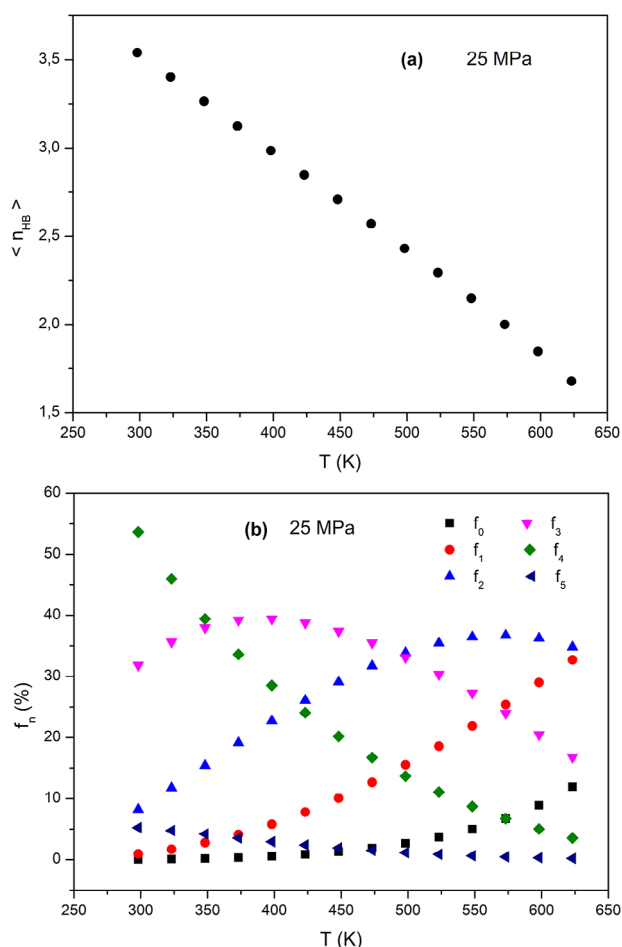


**Figure 5.** Temperature dependence of the mean number of hydrogen bonds per water molecule  $\langle n_{\text{HB}} \rangle$  and the fractions of water molecules  $f_n$  forming  $n = 0-5$  hydrogen bonds.

hydrogen bond between two water molecules exists if the interatomic distances are such that  $R_{\text{O} \dots \text{O}} \leq 3.6 \text{ \AA}$ ,  $R_{\text{H} \dots \text{O}} \leq 2.4 \text{ \AA}$  and the donor-acceptor angle  $\text{H-O} \dots \text{O} \leq 30^\circ$  (the symbol  $\dots$  corresponds to intermolecular distances). Using this criterion, the average number of hydrogen bonds per water molecule  $\langle n_{\text{HB}} \rangle$ , as well as the percentage fractions  $f_n$  of water molecules forming  $n = 0-5$  hydrogen bonds, have been calculated and their temperature dependence is presented in Figure 5.

From Figure 5a it can be clearly observed that as the temperature increases, the mean number of hydrogen bonds per water molecule  $\langle n_{\text{HB}} \rangle$ , decreases almost linearly. At 298.15 K, the value of  $\langle n_{\text{HB}} \rangle$  is 3.54, signifying that the well-known tetrahedral ordering due to the formation of hydrogen bonds is still present in high-pressure liquid water. However, at 623.15 K this value has dropped to 1.68, clearly indicating that the HB network in near-critical high-pressure water has been significantly disrupted.

The fractions of water molecules  $f_n$  forming  $n = 0-5$  hydrogen bonds also change significantly as the temperature increases, as clearly depicted in Figure 5b. At ambient temperature the dominating fraction is  $f_4$ , signifying that indeed the majority of water molecules form four hydrogen bonds with their neighbors.

However, at temperatures higher than 348.15 K the fraction of molecules forming three hydrogen bonds becomes the dominating one and this fraction  $f_3$  increases up to 398.15 K. At 423.15 K the fraction of molecules forming two hydrogen bonds,  $f_2$ , becomes larger than the fraction of molecules forming four hydrogen bonds,  $f_4$ , whereas as the temperature continues to increase the fraction  $f_3$  also starts to decrease rapidly. At 498.15 K the dominating fraction is  $f_2$ , whereas  $f_1$  also becomes higher than  $f_4$ . At temperatures higher than 498.15 K the fraction of hydrogen-bonded free molecules,  $f_0$ , starts to become non-negligible and increases with the temperature increase. At near-critical temperatures (623.15 K) it can be clearly observed that the dominating fractions are  $f_2$  and  $f_1$ , further supporting our previous statement regarding the disruption of the HB network in near-critical high-pressure water. As mentioned above, at ambient conditions liquid water is still characterized by the existence of locally favored tetrahedral structures, due to the formation of hydrogen bonds of the water molecules with their closest neighbors.<sup>[35]</sup> In order to quantify the deviation of the local orientational structural order in liquid water from a perfect tetrahedral order, a tetrahedral order parameter  $q$  has been introduced in the literature.<sup>[16]</sup> This parameter provides information about the extent to which a molecule and its four nearest neighbors adopt a tetrahedral arrangement and is defined as:

$$q = 1 - \left\langle \frac{3}{8} \sum_{j=1}^3 \sum_{k=j+1}^4 \left( \cos \phi_{jik} + \frac{1}{3} \right)^2 \right\rangle \quad (2)$$

In this equation  $\phi_{jik}$  corresponds to the angle formed by the vectors  $\vec{r}_{ij}$  and  $\vec{r}_{ik}$ , connects the oxygen atom of the central molecule  $i$  with the oxygen atoms of two of its four nearest neighbors  $j$ , and  $k$ . Using this definition the parameter  $q$  gets the value  $q = 1$  in a perfect tetrahedral network and the value  $q = 0$  in an ideal gas. In the present study, the temperature dependence of the average orientational tetrahedral order parameter  $q$  is presented, together with the temperature dependence of its derivative  $dq/dT$ , in Figure 6a. An entropic term  $S_q$ ,<sup>[36]</sup> associated with the local tetrahedral order around the water molecules was also calculated from the probability distribution of the tetrahedral order parameter  $f(q)$ :

$$S_q = \frac{3}{2} \cdot \frac{1}{N} k_B \sum_{i=1}^N \ln(1 - q_i) = \frac{3}{2} \cdot k_B \int \ln(1 - q) \cdot f(q) \cdot dq \quad (3)$$

In Equation (3),  $k_B$  is the Boltzmann constant. The temperature dependence of this entropic term  $S_q$  is presented in Figure 6b.

From Figure 6a, it can be clearly observed that the local tetrahedral order around the water molecules is significantly disrupted as the temperature increases, something which is reflected in the significant decay of the tetrahedral order parameter  $q$ . The slope  $dq/dT$  also changes significantly at  $T = 423.15 \text{ K}$  and  $T = 498.15 \text{ K}$ . Note also that our analysis also revealed an inflection point in the  $q(T)$  curve around 498.15 K. Interestingly, a crossover in the  $S_q(T)$  curve can also be clearly observed at  $T = 423.15 \text{ K}$  if someone inspects Figure 6b. All these observations are also in line with our previous findings regarding the

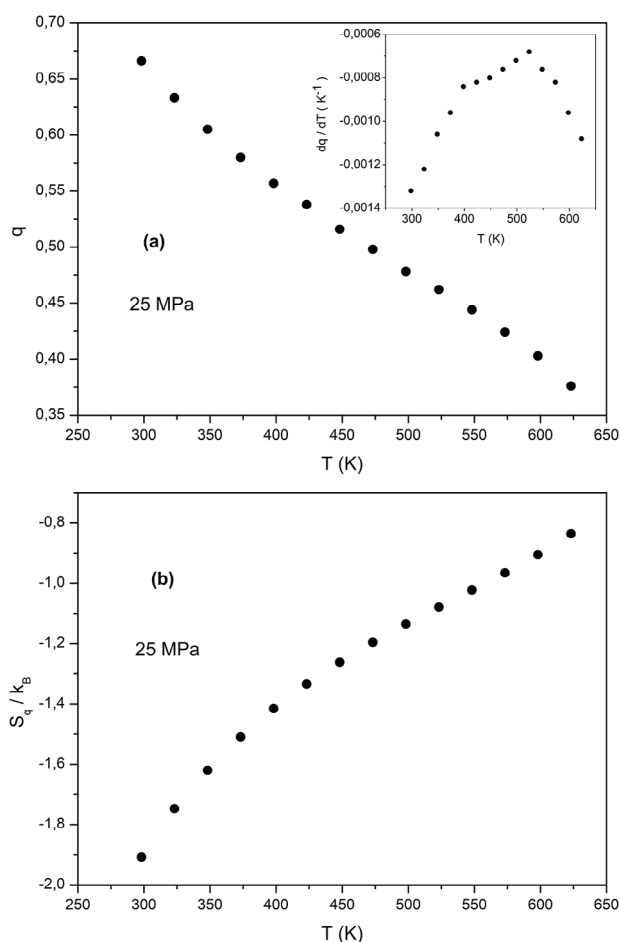


**Figure 6.** Temperature dependence of the average tetrahedral order parameter  $q$  and the corresponding entropic parameter  $S_q$ .

changes in the calculated O-O RDF, the Wendt-Abraham parameter, and the changes in the HB network in high-pressure liquid water, further supporting all the statements related to the structural transitions in liquid water along the 25.0 MPa isobar. The crossover in the  $S_q(T)$  curve at 498.15 K further motivated us to investigate the entropic changes in high-pressure liquid water as the temperature increases from ambient to near-critical values. To do so, we employed the two-phase thermodynamic (2PT) model, which has been presented in detail in previous works in the literature.<sup>[37–39]</sup> Using the 2PT model, the total entropy of liquid water can be calculated. Additionally, in the case of rigid polyatomic molecular systems (like TIP4P-2005 water), the total entropy of the system  $S_{\text{total}}$  can be decomposed into its translational and rotational components  $S_{\text{trans}}$  and  $S_{\text{rot}}$ , respectively. The MD simulation trajectories, containing the atomic positions and velocities, were therefore analyzed using the DoSPT code,<sup>[40]</sup> where the 2PT model is implemented, to calculate the temperature dependence of the total entropy of high-pressure liquid water, as well as of its translational and rotational components and their ratio  $S_{\text{rot}}/S_{\text{trans}}$ . The results obtained are presented in Figures 7 and 8.

As expected, when the temperature increases, both the translational and rotational entropy of water increase. From Figure 7a a crossover in the  $S_{\text{trans}}(T)$  curve is clearly observed

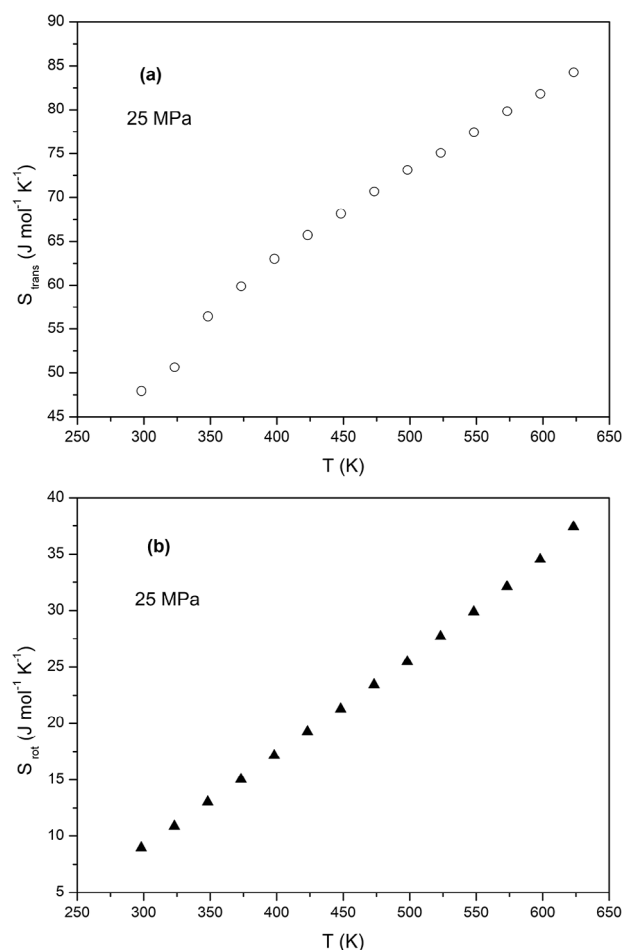


**Figure 7.** Temperature dependence of the translational and rotational entropy of liquid water along the 25 MPa isobar.

around 423.15 K, whereas the dependence of the rotational entropy upon the temperature is almost linear. Interestingly, this crossover is located at the same temperature range where the crossover in the  $S_q(T)$  curve was also observed, signifying that the changes in the local structural order in pressurized high-temperature liquid water are more strongly affecting the translational entropy of the system. The change in the shape of the  $S_{\text{trans}}(T)$  curve is also reflected in the shape of the  $S_{\text{total}}(T)$  curve (Figure 8b). However, the crossover in the latter curve is not as strong as in the case of the  $S_{\text{trans}}(T)$  curve, due to the added rotational entropy component of the total entropy of the system, which has a linear temperature dependence (Figure 7b).

Another interesting observation is that as the temperature increases, the ratio  $S_{\text{rot}}/S_{\text{trans}}$  increases significantly (Figure 8a), indicating that as water approaches the critical point the contribution of rotational motions to the total entropy of the system becomes much more important in comparison with ambient-temperature water.

Recent studies in ambient and supercooled water have revealed the existence of two locally favored structures<sup>[41–43]</sup> when employing a structural order parameter  $\zeta$ , introduced by Russo and Tanaka.<sup>[17,44]</sup> By definition, this order parameter  $\zeta$  of a water molecule corresponds to the difference between its

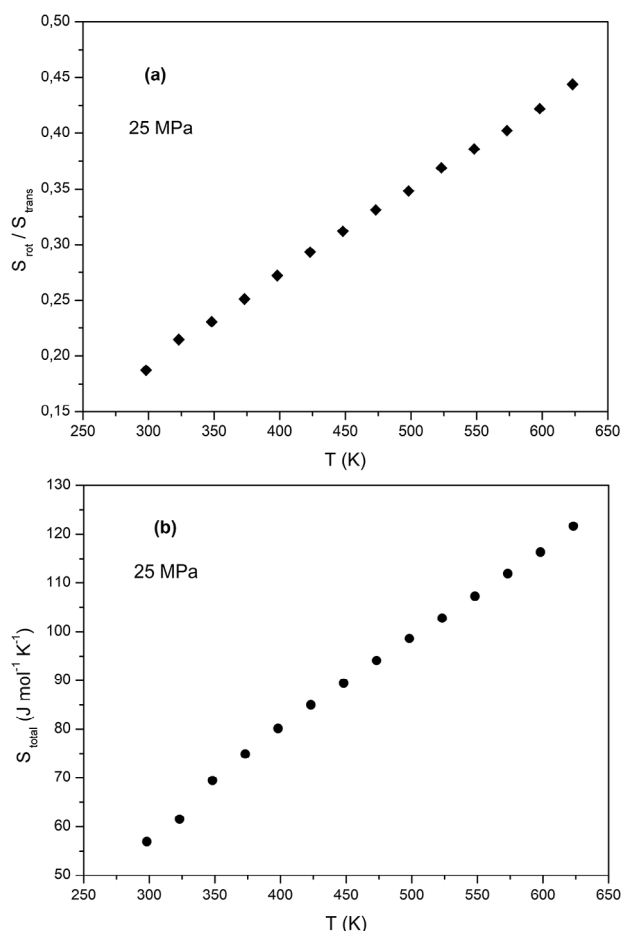


**Figure 8.** Temperature dependence of the ratio  $S_{\text{rot}} / S_{\text{trans}}$  and the total entropy  $S_{\text{total}}$  of liquid water along the 25 MPa isobar.

distance from the nearest non-hydrogen-bonded neighbor and its distance from the furthest hydrogen-bonded neighbor. In the case of ambient or supercooled liquid water, large positive values of  $\zeta$  indicate a sharp separation between the first and second coordination shells. Negative or vanishing values of  $\zeta$  indicate a merging of the second coordination shell with the first.<sup>[41]</sup>

For this reason, apart from the calculation of temperature dependence of the average value of  $\zeta$ , presented in Figure 9a, the fraction of water molecules exhibiting negative  $\zeta$  values was also calculated and presented in Figure 9b. From Figure 9a it can be observed that  $\zeta$  initially decreases with the increase of the temperature and it obtains its minimum value at 498.15 K. At temperatures higher than 498.15 K the values of  $\zeta$  start to increase again. This finding is also in line with our previous observations regarding the structural changes in high-pressure liquid water. The fraction of water molecules exhibiting negative  $\zeta$  values,  $f(\zeta_{\text{negative}})$ , although it's not the dominating one, it increases significantly with the increase of the temperature and reaches its maximum value (0.395) around 548.15 K. At temperatures higher than 548.15 K this fraction slightly decreases.

Apart from the investigation of the thermodynamic and static structural properties of high-pressure liquid water, the

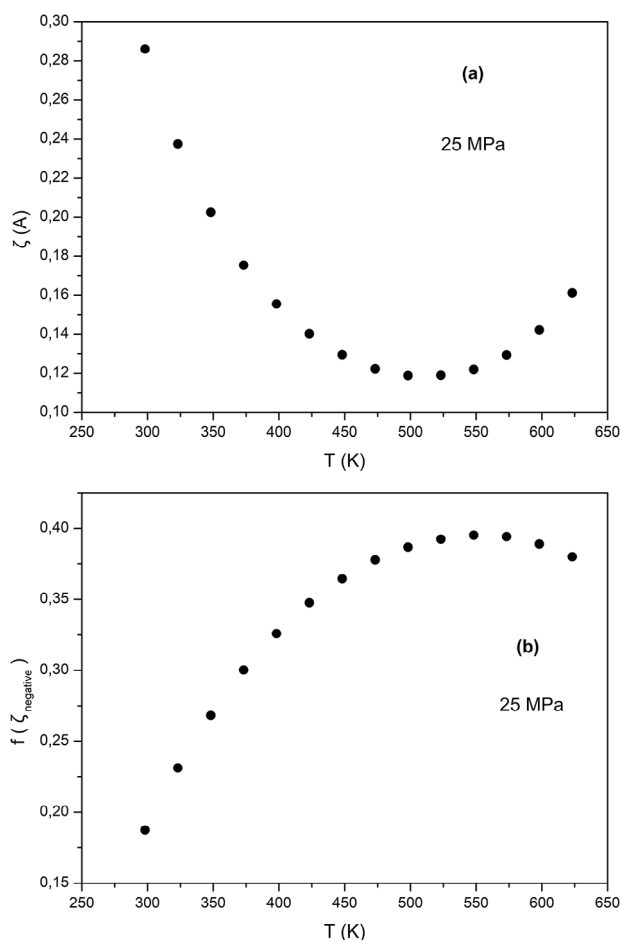


**Figure 9.** Temperature dependence of the average number of  $\zeta$  and the fraction of water molecules exhibiting negative  $\zeta$  values,  $f(\zeta_{\text{negative}})$ .

investigation of the temperature effects upon its dynamic properties was also investigated in the framework of the present study. In this respect, the dynamics of the hydrogen bonds formed among the water molecules were investigated in terms of the corresponding HB time correlation functions (TCF)<sup>[45–47]</sup>:

$$C_{\text{HB}}(t) = \frac{\langle \delta h_{ij}(0) \cdot \delta h_{ij}(t) \rangle_{t^*}}{\langle \delta h_{ij}(0)^2 \rangle}, \quad \delta h_{ij}(t) = h_{ij}(t) - \langle h_{ij} \rangle \quad (4)$$

The variable  $h_{ij}$  is such as  $h_{ij}(t) = 1$  when a specific hydrogen bond between two water molecules  $i, j$  is formed at times 0 and  $t$ , and the corresponding hydrogen bond has not been broken in the meantime for a period longer than  $t^*$ , otherwise,  $h_{ij}(t) = 0$ . The case where  $t^* = 0$  corresponds to the continuous HB dynamics, and the one where  $t^* = \infty$  corresponds to the intermittent HB dynamics. These two definitions describe very different aspects of HB dynamics. According to the continuous definition, the breaking of a hydrogen bond during the time interval  $[0, t]$  is not allowed and the continuous lifetime is the time required for the first breaking of a bond created at time  $t = 0$ .

On the other hand, in the intermittent case, the persistence probability at time  $t$  of a hydrogen bond created at  $t = 0$  is investigated, regardless of multiple breakings and reformations of this



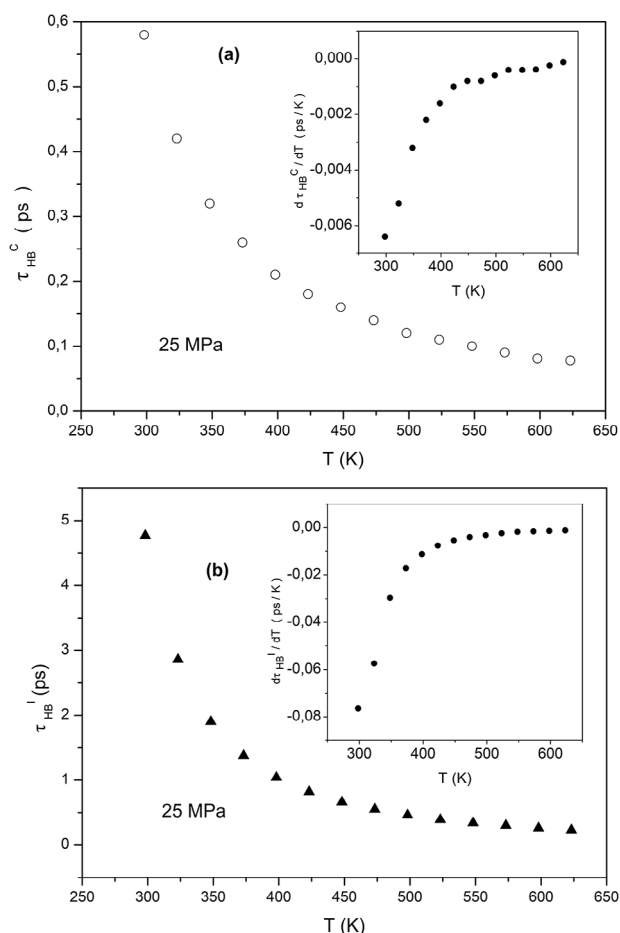


**Figure 10.** Temperature dependence of the continuous and intermittent HB lifetimes of liquid water along the 25 MPa isobar. Their derivatives with respect to temperature are presented in the inset pictures.

bond during the time interval  $[0, t]$ . The calculated TCF in these two different cases are the continuous  $C_{HB}^C(t)$  and intermittent  $C_{HB}^I(t)$  TCF, respectively. As the system size increases  $\langle h_{ij} \rangle \rightarrow 0$  and at the infinite size limit it approaches the zero value. In the case where  $\langle h_{ij} \rangle \simeq 0$  Equation (4) can be expressed as:

$$C_{HB}(t) = \frac{\langle h_{ij}(0) \cdot h_{ij}(t) \rangle_{t^*}}{\langle h_{ij}(0)^2 \rangle} \quad (5)$$

The HB lifetime  $\tau_{HB}$  is defined as:

$$\tau_{HB} = \int_0^\infty C_{HB}(t) \cdot dt \quad (6)$$

The temperature dependence of the calculated continuous,  $\tau_{HB}^C$ , and intermittent,  $\tau_{HB}^I$ , HB lifetimes is presented in Figure 10. From Figure 10 it can be clearly observed that in the temperature range 298.15–423.15 K both the continuous and intermittent HB lifetimes decrease rapidly and then the decay is significantly less rapid, as also very clearly reflected upon their derivatives with respect to temperature, which are presented in the inset figures in Figure 10a and Figure 10b. This crossover observed at 423.15 K in the curves presented in Figure 10 is a strong indica-

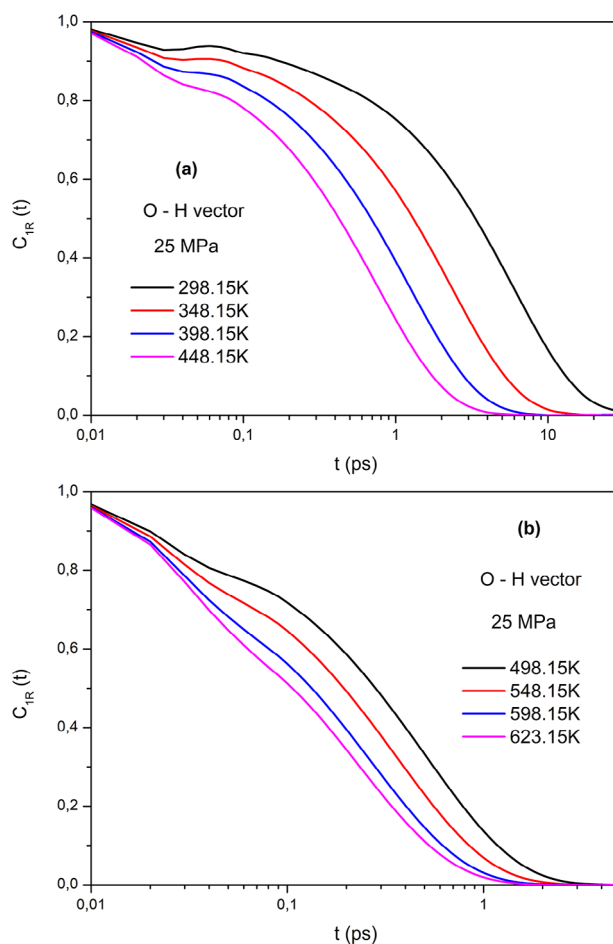


**Figure 11.** Temperature effects on the time decay of the calculated first-order Legendre reorientational TCF for the O-H vectors of the water molecules.

tion of the effect of the structural transitions taking place in this temperature range upon the dynamic properties of the system.

The temperature effects upon the reorientational dynamics of the water molecules were also investigated in the framework of the present study, in terms of the Legendre reorientational TCF<sup>[48,49]</sup>:

$$C_{\ell R}(t) = P_\ell \left( \vec{u}_i(0) \cdot \vec{u}_i(t) \right) \quad (7)$$

In Equation (7),  $\vec{u}_i$  is a unit vector along the O-H vector of water molecules, and  $P_\ell$  is a Legendre polynomial of order  $\ell$ .

The corresponding Legendre reorientational correlation times were calculated using the following equation:

$$\tau_{\ell R} = \int_0^\infty C_{\ell R}(t) \cdot dt \quad (8)$$

The temperature effects upon the shape and decay of the first-order Legendre reorientational TCF for the O-H vectors of the water molecules are presented in Figure 11. A typical characteristic of this reorientational TCF in the case of ambient liquid water is the observation of a local minimum at very short time scales, related to the water rotational motions and the

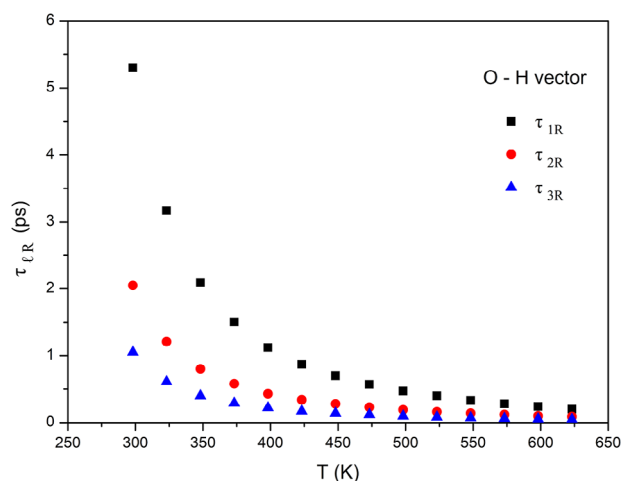


**Figure 12.** Temperature dependence of the calculated first-, second-, and third-order Legendre reorientational correlation times for the O-H vectors of the water molecules.

librations of the O-H vector during the breaking and formation of hydrogen bonds.<sup>[50–53]</sup> As it can be observed in Figure 11, as the temperature increases this short-time scale local minimum becomes less apparent, and at temperatures higher than 498.15 K, it is not observed (Figure 11b). Moreover, it can be clearly observed that particularly in the temperature range 298.15–423.15 K the temperature effects on the decay of the calculated reorientational TCF are very strong. This is also reflected in the calculated reorientational correlation times. In Figure 12 the temperature dependence of the calculated first, second, and third-order Legendre reorientational correlation times is presented. The temperature dependence of these reorientational correlation times is very similar to the one observed for the HB lifetimes, with a crossover observed around 423.15 K. All these findings clearly manifest the strong interrelation between the structural changes and the dynamic properties of liquid water as the temperature goes from ambient to near-critical values.

Finally, the temperature effect on the translational self-diffusion coefficient of the water molecules has been investigated in the present study. The self-diffusion coefficient of water has been calculated using the calculated molecular mean-square displacements (MSD) and the well-known Einstein relation:

$$D = \frac{1}{6} \lim_{t \rightarrow \infty} \frac{1}{t} \left\langle \left| \vec{\Delta r}_i(t) \right|^2 \right\rangle = \frac{1}{6} \lim_{t \rightarrow \infty} \frac{1}{t} \left\langle \left| \vec{r}_i(0) - \vec{r}_i(t) \right|^2 \right\rangle \quad (9)$$

The temperature dependence of the self-diffusion coefficient of water is presented in Figure 13.

The activation energy for the translational self-diffusion of water was estimated by fitting an Arrhenius equation to the calculated self-diffusion data:

$$\ln D = \ln D_0 - \frac{E_a}{RT} \quad (10)$$

In Equation (10),  $D_0$  is a pre-exponential factor and  $R$  is the ideal gas constant. The calculated activation energy for translational self-diffusion along the 25 MPa isobar has been found to be 3.38 kcal mol<sup>−1</sup>. A similar procedure was followed as

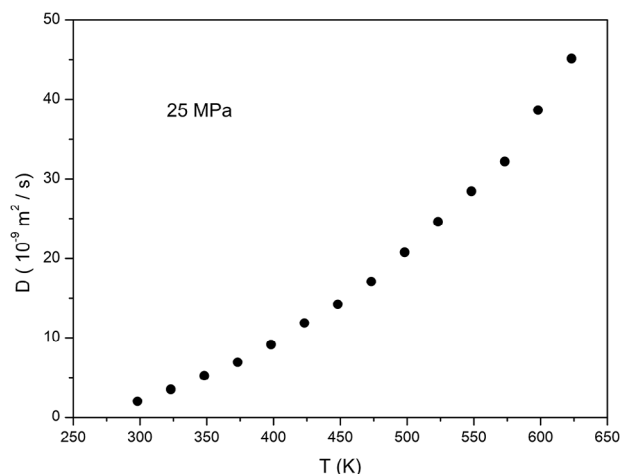


**Figure 13.** Temperature dependence of the calculated translation self-diffusion of liquid water along the 25 MPa isobar.

**Table 1.** Calculated activation energies for translational diffusion, molecular reorientation, and intermittent-continuous HB dynamics along the 25 MPa isobar in the temperature range 298.15–623.15 K.

Process (Quantity under study)	$E_a$ (kcal mol <sup>−1</sup> )
Translational Diffusion ( $D$ )	3.38
O-H Reorientation ( $\tau_{1R}^{OH}$ )	3.60
Intermittent HB Dynamics ( $\tau_{HB}^{(I)}$ )	3.36
Continuous HB Dynamics ( $\tau_{HB}^{(C)}$ )	2.27

well in the case of reorientational dynamics and intermittent-continuous HB dynamics. An Arrhenius equation was fitted to the calculated temperature dependence of the first-order Legendre reorientational correlation time for the O-H vector and the intermittent and continuous HB lifetimes. The calculated activation energies for each process are presented in Table 1.

From the results presented in Table 1, it can be clearly seen that the activation energies for translational self-diffusion, molecular reorientational dynamics, and intermittent HB dynamics are quite similar. This finding is not surprising, since it is well-known that there is a strong interrelation between translational, reorientational, and intermittent HB relaxation dynamics in liquid water. On the other hand, the continuous HB dynamics is only related to the first breaking of a hydrogen bond and is characterized by a lower activation energy. This finding is also reasonable since the intermittent HB relaxation dynamics is related to multiple breakings and reformations of a hydrogen bond until an initially hydrogen-bonded pair loses any kind of structural correlation. In this respect, the activation energy of such a process should be higher in comparison with continuous HB dynamics.

## 4. Conclusions

In the framework of the present study, classical molecular dynamics simulations of liquid water were performed along the



25 MPa isobar and in the temperature range 298.15–623.15 K Particular attention has been given to the temperature effects upon the local structural order and the HB network, as reflected upon the changes of the calculated RDF, the average numbers of hydrogen bonds per water molecule and related HB statistics, as well as on several well-established structural order parameters. The results obtained have revealed noticeable changes in the shape of the calculated RDF, as well as the existence of local extrema or crossovers in several structural descriptors and entropic quantities at temperatures around 423.15 K and 498.15 K. Interestingly, in the above-mentioned temperature range, significant changes in the hydrogen bond network of liquid water have also been observed. The investigation of the temperature effects upon the translational, reorientational, and hydrogen bond dynamics of liquid water has also revealed the existence of crossovers around 423.15 K. The results obtained also revealed the disappearance of a local minimum in the reorientational TCF of the O-H vector of water molecules at very short time scales, related to the water rotational motions during the breaking and formation of hydrogen bonds, at temperatures higher than 498.15 K. All these findings are strong evidence of the interplay between the structural transitions and several relaxation phenomena in high-pressure liquid water as the temperature goes from ambient to near-critical values.

## Acknowledgements

The use of the computational facilities of the *Computer Simulation in Condensed Matter Research Group* (SIMCON) in the Department of Physics, Polytechnic University of Catalonia (UPC) is gratefully acknowledged., E.G., acknowledges the financial support from the Ministerio de Ciencia e Innovación of Spain, Grant No. PID2021-124297NB-C32 and the financial support from the Generalitat de Catalunya (Grant No. 2021 SGR 01411).

## Conflict of Interests

The authors declare no conflict of interest.

## Data Availability Statement

The data that support the findings of this study are available from the corresponding author upon reasonable request.

**Keywords:** high pressure · high temperature · liquid water · molecular dynamics · structural transitions

- [1] J. Szala-Blinik, D. Sviatla-Wojcik, *J. Mol. Liq.* **2011**, *164*, 34.
- [2] A. Kruse, E. Dinjus, *J. Supercrit. Fluids* **2007**, *39*, 362.
- [3] P. E. Savage, *J. Supercrit. Fluids* **2009**, *47*, 407.
- [4] N. Akiya, P. E. Savage, *Chem. Rev.* **2002**, *102*, 2725.
- [5] A. R. Katritzky, S. M. Allin, M. Siskin, *Acc. Chem. Res.* **1996**, *29*, 399.
- [6] Y. Cheng, F. Xue, S. Yu, S. Du, Y. Yang, *Molecules* **2021**, *26*, 4004.
- [7] Y. Yang, *J. Sep. Sci.* **2007**, *30*, 1131.

- [8] J. Zhang, C. Wen, H. Zhang, Y. Duan, H. Ma, *Food Sci. Technol.* **2020**, *95*, 183.
- [9] Y. Yang, S. B. Hawthorne, D. J. Miller, *Environ. Sci. Technol.* **1997**, *31*, 430.
- [10] F. Chemat, M. A. Vian, G. Cravotto, *Int. J. Mol. Sci.* **2012**, *13*, 8615.
- [11] C. C. Teo, S. N. Tana, J. W. Yong, C. S. Hew, E. S. Ong, *J. Chromatogr. A* **2010**, *1217*, 2484.
- [12] R. M. Smith, *J. Chromatogr. A* **2008**, *1184*, 441.
- [13] A. H. Harvey, D. G. Friend in *Aqueous systems at elevated temperatures and pressures: Physical chemistry in water, steam and hydrothermal solutions* (Eds.: D. A. Palmer, R. Fernández-Prini, A. H. Harvey), Elsevier, Amsterdam, The Netherlands, **2004**, pp. 1–27.
- [14] M. P. Allen, D. J. Tildesley, in *Computer Simulations of Liquids*, Oxford University Press, Oxford, UK, **1987**.
- [15] J. L. F. Abascal, C. Vega, *J. Chem. Phys.* **2005**, *123*, 234505.
- [16] J. R. Errington, P. G. Debenedetti, *Nature* **2001**, *409*, 318.
- [17] J. Russo, H. Tanaka, *Nat. Commun.* **2014**, *5*, 3556.
- [18] L. Martínez, R. Andrade, E. G. Birgin, J. M. Martínez, *J. Comput. Chem.* **2009**, *30*, 2157.
- [19] C. Vega, J. L. F. Abascal, I. Nezbeda, *J. Chem. Phys.* **2006**, *125*, 034503.
- [20] W. G. Hoover, *Phys. Rev. A* **1985**, *31*, 1695.
- [21] W. G. Hoover, *Phys. Rev. A* **1986**, *34*, 2499.
- [22] W. Smith, T. R. Forester, *J. Mol. Graph.* **1996**, *14*, 136.
- [23] W. Wagner, A. Pruss, *J. Phys. Chem. Ref. Data* **2002**, *31*, 387.
- [24] P. A. Egelstaf, in *An Introduction to the Liquid State*, Academic Press, London, UK, **1967**.
- [25] J.-P. Hansen, I. R. McDonald, in *Theory of Simple Liquids*, Academic Press, Oxford, UK, **2006**.
- [26] C. G. Gray, K. E. Gubbins, in *Theory of Molecular Fluids*, Oxford University Press, Oxford, UK, **1984**.
- [27] A. K. Soper, *Chem. Phys.* **2000**, *258*, 21.
- [28] H. R. Wendt, F. F. Abraham, *Phys. Rev. Lett.* **1978**, *41*, 1244.
- [29] J. Marti, *J. Chem. Phys.* **1999**, *110*, 6876.
- [30] C. Nieto-Draghi, J. Bonet Avalos, B. Rousseau, *J. Chem. Phys.* **2003**, *118*, 7954.
- [31] I. Skarmoutsos, E. Guardia, *J. Chem. Phys.* **2010**, *132*, 074502.
- [32] I. Skarmoutsos, A. Henao, E. Guardia, J. Samios, *J. Phys. Chem. B* **2021**, *125*, 10260.
- [33] I. Skarmoutsos, E. Guardia, J. Samios, *J. Supercrit. Fluids* **2017**, *130*, 156.
- [34] I. Skarmoutsos, D. Dellis, J. Samios, *J. Phys. Chem. B* **2009**, *113*, 2783.
- [35] D. Eisenberg, W. Kauzmann, in *The Structure and Properties of Water*, Oxford University Press, New York, USA, **1969**.
- [36] P. Kumar, S. V. Buldyrev, H. E. Stanley, *Proc. Natl. Acad. Sci. U.S.A.* **2009**, *106*, 22130.
- [37] S.-T. Lin, M. Blanco, W. A. Goddard III, *J. Chem. Phys.* **2003**, *119*, 11792.
- [38] S.-T. Lin, P. K. Maiti, W. A. Goddard III, *J. Phys. Chem. B* **2010**, *114*, 8191.
- [39] I. Skarmoutsos, J. Samios, E. Guardia, *J. Phys. Chem. Lett.* **2022**, *13*, 7636.
- [40] M. A. Caro, T. Laurila, O. Lopez-Acevedo, *J. Chem. Phys.* **2016**, *145*, 244504.
- [41] I. Skarmoutsos, G. Franzese, E. Guardia, *J. Mol. Liq.* **2022**, *364*, 119936.
- [42] R. Shi, H. Tanaka, *J. Am. Chem. Soc.* **2020**, *142*, 2868.
- [43] R. Shi, J. Russo, H. Tanaka, *J. Chem. Phys.* **2018**, *149*, 224502.
- [44] H. Tanaka, H. Tong, R. Shi, J. Russo, *Nat. Rev. Phys.* **2019**, *1*, 333.
- [45] I. Skarmoutsos, I. D. Petsalakis, J. Samios, *Ind. Eng. Chem. Res.* **2021**, *60*, 11834.
- [46] J. A. Padro, L. Saiz, E. Guardia, *J. Mol. Struct.* **1997**, *416*, 243.
- [47] F. W. Starr, J. K. Nielsen, H. E. Stanley, *Phys. Rev. E* **2000**, *62*, 579.
- [48] B. J. Berne, R. Pecora, in *Dynamic Light Scattering*, Dover Publications, Mineola, NY, USA, **2013**.
- [49] D. Laage, J. T. Hynes, *J. Phys. Chem. B* **2008**, *112*, 14230.
- [50] E. Guardia, I. Skarmoutsos, M. Masia, *J. Phys. Chem. B* **2015**, *119*, 8926.
- [51] D. Laage, J. T. Hynes, *Chem. Phys. Lett.* **2006**, *433*, 80.
- [52] R. Ludwig, *ChemPhysChem* **2007**, *8*, 44.
- [53] D. E. Moilanen, E. E. Fenn, Y.-S. Lin, J. L. Skinner, B. Bagchi, M. D. Fayer, *Proc. Natl. Acad. Sci. U.S.A.* **2008**, *105*, 5295.

Manuscript received: February 1, 2025

Revised manuscript received: March 31, 2025

Version of record online: April 21, 2025